Objective measurement of accommodative biometric changes using ultrasound biomicroscopy

Viswanathan Ramasubramanian, PhD, Adrian Glasser, PhD

PURPOSE: To demonstrate that ultrasound biomicroscopy (UBM) can be used for objective quantitative measurements of anterior segment accommodative changes.

SETTING: College of Optometry, University of Houston, Houston, Texas, USA.

DESIGN: Prospective cross-sectional study.

METHODS: Anterior segment biometric changes in response to 0 to 6.0 diopters (D) of accommodative stimuli in 1.0 D steps were measured in eyes of human subjects aged 21 to 36 years. Imaging was performed in the left eye using a 35 MHz UBM (Vumax) and an A-scan ultrasound (A-5500) while the right eye viewed the accommodative stimuli. An automated Matlab image-analysis program was developed to measure the biometry parameters from the UBM images.

RESULTS: The UBM-measured accommodative changes in anterior chamber depth (ACD), lens thickness, anterior lens radius of curvature, posterior lens radius of curvature, and anterior segment length were statistically significantly linearly correlated with accommodative stimulus demands. Standard deviations of the UBM-measured parameters were independent of the accommodative stimulus demands (ACD: 0.0176 mm; lens thickness: 0.0294 mm; anterior lens radius of curvature: 0.3350 mm; posterior lens radius of curvature: 0.1580 mm; and anterior segment length: 0.0340 mm). The mean difference between the A-scan and UBM measurements was −0.070 mm for ACD and 0.166 mm for lens thickness.

CONCLUSIONS: Accommodating phakic eyes imaged using UBM allowed visualization of the accommodative response, and automated image analysis of the UBM images allowed reliable, objective, quantitative measurements of the accommodative intraocular biometric changes.

Financial Disclosure: Neither author has a financial or proprietary interest in any material or method mentioned.

J Cataract Refract Surg 2015; 41:511–526 © 2015 ASCRS and ESCRS

Accommodation is the ocular dioptric change in refraction in response to ciliary muscle contraction that allows the young distance-corrected eye to focus on near objects.[1] This change in refraction, the accommodative optical response, occurs through changes in the ocular anterior segment structures. During accommodation, the anterior chamber depth (ACD) decreases,[2–4] the lens thickness (LT) increases,[3–5] the lens equatorial diameter decreases,[6,7] the anterior lens radius of curvature and posterior lens radius of curvature decrease,[8–10] and the posterior lens surface moves posteriorly. The ocular accommodative biometric changes have been studied extensively in humans[4,7,8,11] and monkeys,[2,12] and most studies are in agreement with the accommodative biometric changes described above, except for the accommodative movements of the posterior lens surface. Studies report anterior movement,[13,14] posterior movement,[2,3,9,15] or no movement[8,16] of the posterior lens surface during accommodation.

Anterior segment biometric changes during accommodation have been measured using A-scan ultrasound (US),[3,17–19] ultrasound biomicroscopy (UBM),[20,21] optical coherence tomography (OCT),[5,22] partial coherence interferometry (PCI),[4,15] Scheimpflug photography,[9] and magnetic resonance imaging (MRI).[7,8,11] A-scan US and PCI provide quantitative

information about axial biometry but do not allow visualization of the anterior segment, whereas MRI, UBM, OCT, and Scheimpflug photography capture images of the anterior segment and allow both visualization and quantitative measurement of the anterior segment structures. Although MRI has been used to measure accommodative changes in the ocular anterior segment,[7,8] the imaging times are long (seconds to minutes) and the image resolution is limited (0.156 mm).[8] Optical coherence tomography captures images more rapidly (microseconds to milliseconds) and with a resolution of a few microns.[22] Optical imaging methods such as OCT and Scheimpflug photography offer higher resolution than MRI and UBM; however, the optical interfaces preceding the surfaces being measured create optical distortions that require correction for accurate measurements to be made.[9,23] Although optical correction of the posterior corneal surface and the anterior lens surface from refraction by the preceding optical surfaces might be relatively straightforward, accurate optical correction of the crystalline lens posterior surface requires detailed knowledge of the lens gradient refractive index.[23]

Ultrasound biomicroscopy is a clinical method that is widely used to image the anterior segment of the eye in diagnosing and managing conditions such as glaucoma and uveal tumors.[24] The advantages of UBM over other current commercially available clinical anterior segment imaging instruments such as OCT include a deeper signal penetration, the ability to image structures covered by the iris, and an absence of the optical distortions that are inherent in optical ocular imaging methods. Ultrasound biomicroscopy also acquires images as video sequences that can be used to perform multiple measurements. Disadvantages of UBM include a limited image resolution and that it is relatively more invasive, requiring use of a topical anesthesia, a scleral cup, and a fluid interface in front of the eye.

Submitted: April 29, 2014.
Final revision submitted: August 6, 2014.
Accepted: August 8, 2014.

From the College of Optometry, University of Houston, Houston, Texas, USA.

Supported by the National Institutes of Health/National Eye Institute R01 EY017076 (Dr. Glasser) and National Institutes of Health/National Eye Institute P30 EY07551, Bethesda, Maryland, USA (Core Grant to the University of Houston College of Optometry).

Sonomed Escalon provided the ultrasound biomicroscope, and Chris Kuether, Charles Neff, Jason Marsack, and Jim Elswick provided technical assistance.

Corresponding author: Adrian Glasser, PhD, College of Optometry, University of Houston, 4901 Calhoun Road, Houston, Texas 77204, USA. E-mail: aglasser@uh.edu.

Visualizing and measuring ocular accommodative biometric changes is important for understanding how the eye undergoes accommodation and for understanding the design and evaluation of accommodative restoration strategies. While ocular imaging methods allow visualization of the accommodative structures, their true strength becomes evident when objective measurements can be made from the images. Accurate, objective biometric measurements are useful to evaluate accommodation in pseudophakic eyes with accommodating intraocular lenses (IOLs), for assessment of accommodating IOL design, performance, and limitations. In addition, because accommodative biometric changes and the objectively measured accommodative optical response have been shown to be linearly correlated,[2–4,6] objective measures of biometry can be used to predict the accommodative optical response. Per diopter changes in biometry calculated from stimulus amplitudes rather than from objectively measured accommodative optical response amplitudes underestimate the actual per diopter biometry changes because the actual accommodative response lags behind the stimulus amplitude.[2,25] However, because previous accommodation biometry studies[9,14,17,19] report per diopter of stimulus amplitude values, for comparison, this study does as well. Although previous UBM studies have reported measurements of various anterior segment parameters (distances and angles) that might change during accommodation,[20,21] to our knowledge none has used objective image analysis methods with the UBM images. In these studies, manual measurement was performed by 1 or more examiners using software calipers, and only 1[21] or 2[20] individual UBM images were measured.

In the present study, UBM was used to image accommodative biometric changes in the ocular anterior segment in young phakic human eyes. An automated Matlab (The Mathworks) image analysis program was developed to perform objective measurements on sequences of captured UBM images. The UBM measurements were compared with similar measurements made using A-scan US. Slopes of the accommodative stimulus–response functions of different anterior segment parameters in the current study were compared with values from previous anterior segment imaging studies.

SUBJECTS AND METHODS

Subjects

The study followed the tenets of Declaration of Helsinki and was performed in accordance with an institutionally approved human subject protocol. All subjects signed an informed consent document and completed a visual history questionnaire. Exclusion criteria included a spherical

refractive error greater than ±6.0 diopters (D), astigmatism greater than 2.0 D, a history of ocular surgery or ocular disease, and known sensitivity or other contraindication to the topical anesthetic (proparacaine hydrochloride 0.5% [Eye Caine]). Preliminary screening was performed, which included measurement of uncorrected baseline refraction, subjective refraction, and anterior segment evaluation using slitlamp biomicroscopy. Cycloplegic refraction with tropicamide 1.0% was performed in hyperopic eyes (those having a baseline refraction greater than +0.50 D). Subjects with refractive errors were corrected using spherical or toric soft contact lenses.

Ultrasound Biomicroscopy

Because subjects had to lie on their backs and look upward during the UBM imaging, an aluminum frame was constructed (Item North America) to hold a mirror for viewing a far target and a beam splitter for viewing a near target (Figure 1, *A*). The frame was adjustable to allow the correct positioning of these components. A projected far letter target was viewed at 6 m, reflected off a plane mirror inclined at 45 degrees. The near target was a custom-designed, illuminated near-letter chart that the subject's right eye viewed as a reflection off a beam splitter. The near target could be moved on a meter stick to change the target vergence from 1.0 to 6.0 D in 1.0 D steps. In addition, the meter stick could be rotated around a pivot point to alter the angle of gaze of the 2 eyes.

Anterior segment accommodative changes in the left eye were imaged using UBM (Vumax, Sonomed Escalon). The subject was supine on a reclining clinic examination chair with his or her head stabilized using a gel headrest (Figure 1, *B*). Before imaging, the contact lens, if present, was removed from the left eye. Two drops of proparacaine hydrochloride 0.5% were instilled in the left eye, and a scleral eyecup was inserted under the eyelids and filled with warmed balanced salt solution (BSS, Alcon Laboratories, Inc.). All UBM imaging was performed in dim room illumination. Three sequences of 50 well-aligned anterior segment UBM images of the left eye were captured over 8 seconds using a 35 MHz transducer while the subject accommodated to each stimulus demand from 0 to 6.0 D in 1.0 D steps. All UBM scans were of the horizontal ocular meridian (from 3 to 9 o'clock).

For each stimulus demand, the subject adjusted the angle of the near target on the meter stick so that the right eye took up all of the accommodative convergence as determined by the examiner and the left eye remained in the primary gaze posture. The UBM transducer was aligned by ensuring an absence of tilt of the iris plane in the UBM image and by imaging a plane of the section of the eye that provided the largest pupil diameter (Figure 1, *C*). Adequate distance of the anterior corneal surface from the top of the UBM scan window was maintained to ensure that UBM corneal distortion artifacts were avoided.

Image Analysis

Horizontal and vertical spatial pixel-to-mm calibration factors for the UBM images were calculated by imaging a saw-toothed acrylic calibration block of known dimensions. The peaks and valleys of the saw-toothed block were manually marked on the UBM images, from which distances were measured (Figure 1, *D*). The means of horizontal and vertical pixel-to-mm conversion factors calculated from 20 images were 54.60 ± 1.38 pixels/mm and 51.20 ± 1.02 pixels/mm, respectively.

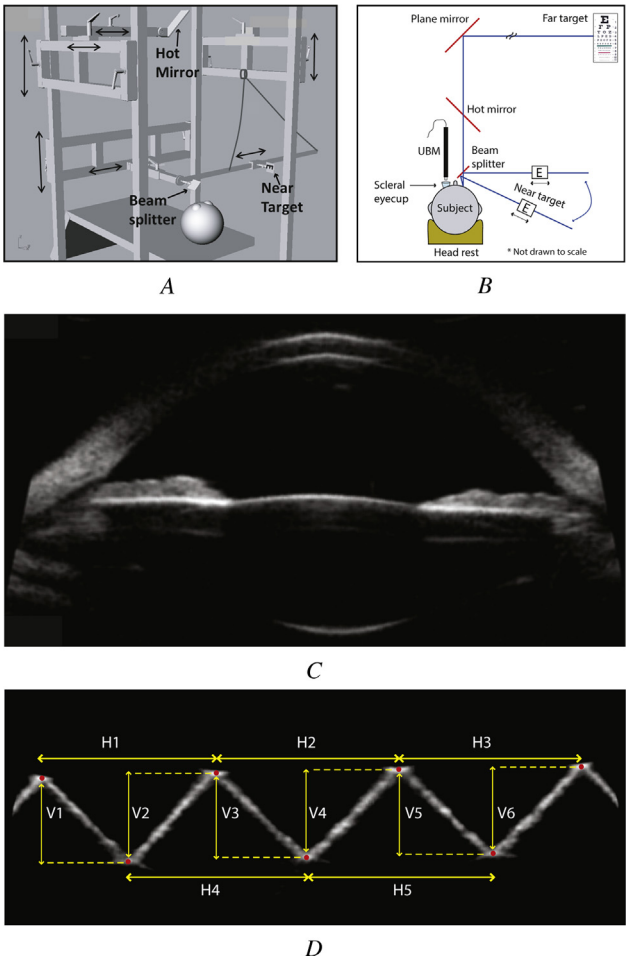

Figure 1. *A*: The aluminum frame for holding various optical components and for stimulating accommodation. *B*: Experimental setup for UBM in the left eye while the right eye views the near or far target. *C*: A raw UBM image of an eye in an unaccommodated state. *D*: The UBM image of the acrylic calibration block with red points marked. Yellow arrows indicate the distances measured from the images (H = horizontal; V = vertical).

All captured UBM images were analyzed offline using custom-developed automated Matlab image analysis software. The program loaded the first of a sequence of 50 UBM video images and required the user to make 2 mouse clicks, 1 in the vicinity of each of the vertices of the anterior chamber angles in the first image. This was the only user input required, and the software performed all further analysis on the 50 images automatically as follows: The gray-scale UBM image was converted to a black-and-white binary image using an automatically determined threshold. A 20 pixel × 20 pixel region of interest around each of the marked points was used to find the left and right anterior chamber angle vertices, from which the angle-to-angle (ATA) distance was calculated. The 2 angle x, y-coordinate vertices served as the starting points for tracing up to a maximum of 80 boundary pixels along the anterior surface of the iris and a maximum of 80 pixels along the posterior corneal surface. The number of boundary pixels from each trace was automatically determined by finding the smallest mean square deviation of the pixels from a segmented linear regression that progressively increased in length. The left and right

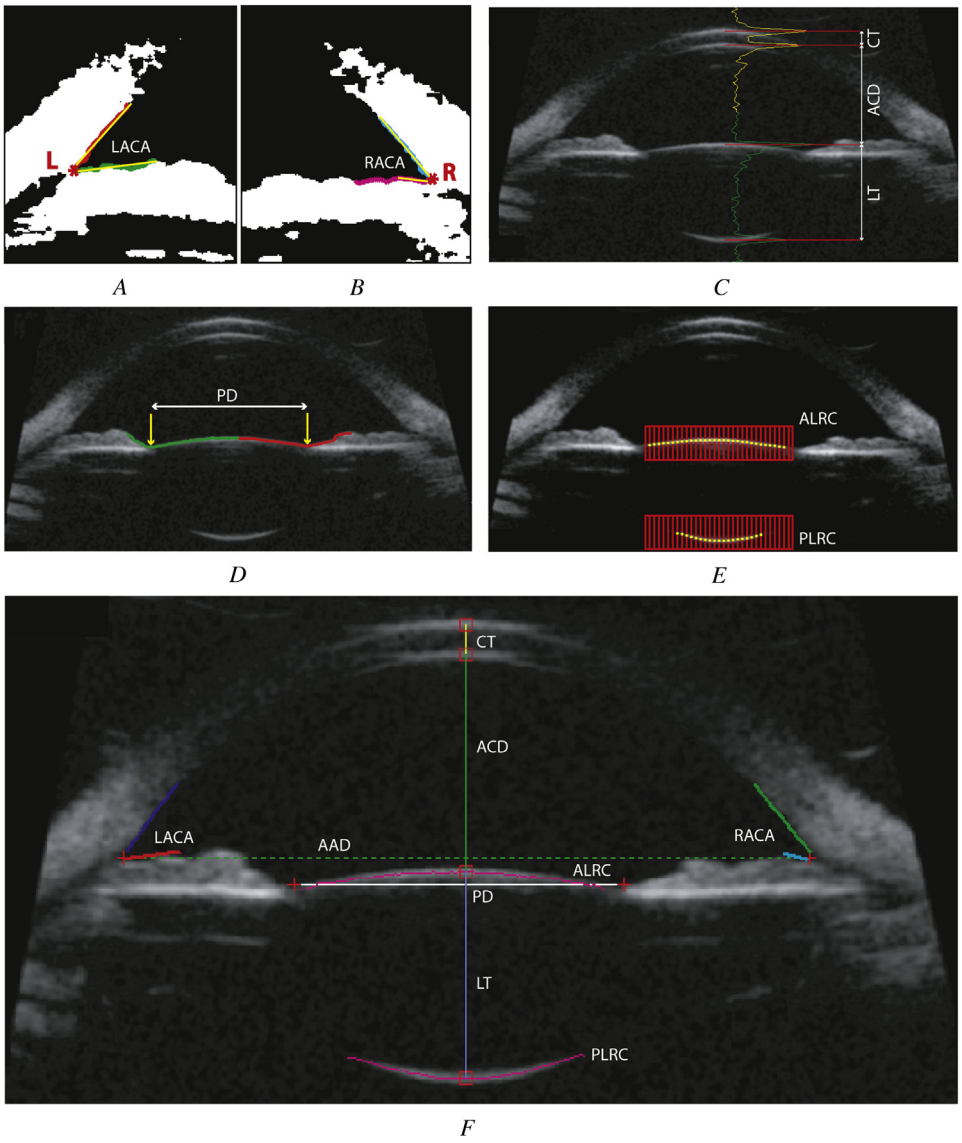

Figure 2. The left (*A*) and right (*B*) anterior chamber angles were calculated from individual regression lines (*yellow*) fitted to the traced corneal and iris edge points (*red, green, cyan, and magenta*). Asterisks represent the vertices of the left and right anterior chamber angles. *C*: Axial biometric distances were calculated from the peaks of the luminance profiles (*yellow and green*). *D*: Pupil diameter is represented by the distance between the *x*-coordinates with the largest *y*-coordinates of the 2 contour traces (*yellow arrows* on *red* and *green boundaries*). *E*: Lens surface points (*yellow*) were detected using the peak of luminance profiles along each vertical red line within the 2 red search regions of interest. For clarity, only subsets of the vertical lines (*red*) are shown. *F*: Ultrasound biomicroscopy image showing all analyzed measurements (AAD = angle-to-angle distance; ACD = anterior chamber depth; ALRC = anterior lens radius of curvature; CT = corneal thickness; LACA = left anterior chamber angle; LT = lens thickness; PD = pupil diameter; PLRC = posterior lens radius of curvature; RACA = right anterior chamber angle).

anterior chamber angles were determined as the angle between the 2 resultant linear regression lines (Figure 2, *A* and *B*). If the left- and right-angle *y*-coordinates were different, the angle of the line connecting them was determined and the gray-scale UBM image was rotated by this angle to correct for tilt in the image. The rest of the analysis was performed on the rotated gray-scale image. The midpoint of the *x*-coordinates of the 2 angle vertices was considered to be the axis of symmetry in the eye. All axial biometry measurements were made vertically along this axis. The luminance profile along this axis was extracted, and the maxima of each of the 4 peaks corresponding to the vertex positions of the anterior and posterior surfaces of the cornea and the lens were determined. Corneal thickness, ACD, and lens thickness were calculated from the distances between the peaks (Figure 2, *C*).

The *x*- and *y*-coordinates of the vertex of the anterior lens surface served as the starting point for tracing up to a maximum of 200 pixels along the anterior surface of the lens and the iris on either side of the vertex. The pupil diameter was identified as the distance between the 2 *x*-coordinates with the largest *y*-coordinates of the 2 traced contours (Figure 2, *D*). To identify the anterior lens surface, a region of interest containing the anterior lens surface was automatically extracted. The region's width was 10 pixels less than the identified pupil diameter, and its height was 40 pixels. Another 200 pixel × 40 pixel region of interest was extracted from around the posterior lens surface vertex. The anterior and posterior lens surface coordinates were determined to be the maxima of the peaks of the luminance profiles along each vertical line of pixels within the regions of interest. The number of luminance lines equaled the width of the regions of interest. Figure 2, *E*, shows a subset of these luminance lines with the maxima. All of the lens anterior and independently the posterior surface coordinates were fit with circles to obtain the radii of curvature. These represent the anterior lens radius of curvature and the posterior lens radius of curvature. Figure 2, *F*, shows the complete analysis of a single UBM image with all measured parameters.

The automated analysis of the remaining 49 images proceeded as described above without further user intervention using the angle coordinate points from the first of the sequence of 50 UBM images as the starting point for angle

Table 1. Parameters of the calibration surfaces.

Calibration Surface	Radius of Curvature (mm)
Convex surface	
Acrylic ball 01	9.51
Contact lens 01	8.30
Contact lens 02	7.80
Contact lens 03	7.50
Contact lens 04	7.30
Concave surface	
Contact lens 01	7.50
Contact lens 02	7.00
Contact lens 03	6.52
Contact lens 04	6.30
Contact lens 05	6.13

coordinate search regions of interest in the second UBM image. The anterior segment length was calculated as the distance from the first corneal vertex to the posterior lens vertex (including the corneal thickness, the ACD, and the lens thickness). The anterior lens surface movement was defined as the accommodative change in the ACD, and posterior lens surface movement was defined as the accommodative change in anterior segment length. The mean ± standard deviation (SD) of the measured parameters was calculated for each accommodative stimulus demand for the 150 analyzed images.

Calibration of Ultrasound Biomicroscopy Images

The anterior and posterior lens surface radii of curvature were outside the range expected for lens anterior and posterior surfaces. It was determined that the measured radius of curvature was dependent on the *y*-position of the surface in the UBM image because of image distortion. To correct for this distortion, convex and concave calibration surfaces with known radii of curvature approximating the expected range of lens surface curvatures (Table 1) were imaged at various distances from the UBM transducer. The transducer was clamped to a miniature optical rail (M-MRL-6M, Newport Corp.), which allowed precise vertical positioning of it. Fifty images were captured for each calibration surface at each position relative to the transducer. Each UBM image measured 1024 pixels × 512 pixels; a pixel position of ($x = 1$, $y = 1$) represented the top left corner of an image. In each image, the calibration surface coordinates were identified using a custom automated Matlab image analysis program (Figure 3, *A* and *B*). Circles were fitted to 174 pixel coordinates for the convex surface and 138 for the concave surface, and the radius of curvature was calculated. The *y*-vertex position of the surface in the image was determined and marked. The *y*-vertex positions for the convex and concave surfaces in the images ranged from 210 to 329 pixels and from 390 to 509 pixels, respectively. This corresponded to the position ranges of the anterior and posterior crystalline lens surfaces of imaged subjects in uncalibrated UBM images.

Figure 3 shows the calibration functions for the convex (*C*) and concave (*D*) surfaces of a single contact lens imaged at various distances from the transducer. The *y*-vertex position that corresponded to the actual radius of curvature was calculated using the calibration functions for each calibration surface. The slopes of the convex and concave surface calibration functions were similar for all calibration surfaces. From the graphs, the mean ± SD of the *y*-vertex image position from each calibration surface that yielded the correct actual radius of curvature for the convex and the concave surfaces was 288.50 ± 4.74 pixels and 383.14 ± 8.79 pixels, respectively.

Figure 3 shows the calibration functions for the convex (*E*) and concave (*F*) calibration surfaces with cumulative linear regressions fitted. These calibration graphs show that the radius of curvature of any surface is accurate in the UBM image if the surface is imaged at a particular *y*-position in the UBM image; ie, at the focus. If a surface is imaged above or below the focus, the radius of curvature of the surface must be corrected by some amount (a delta radius) that is directly proportional to the distance in pixels that the surface is from the focus (the delta *y*-vertex position). For each surface imaged, the calibration function (Figure 3, *E* and *F*) was used with the delta *y*-vertex position to calculate the delta radius (ie, the correction factor). Convex and concave calibration surface radii of curvature were corrected using the calculated correction factors. The *y*-vertex focus positions calculated from the cumulative linear regression lines (Figure 3, *E* and *F*) for the convex surface (288.14 pixels) and the concave surface (384.68 pixels) were similar to the mean calculated *y*-vertex positions mentioned above. The subjects' anterior and posterior lens radii of curvature were also corrected in this way. All data shown are distortion-corrected as described.

A-Scan Ultrasound

To provide a comparison for the measurements obtained through the automated UBM image analysis, the axial biometric changes during accommodation were also independently measured in 24 subject eyes using A-scan US (A-5500, Sonomed Escalon) in the left eye while the subject remained supine. Two drops of proparacaine hydrochloride 0.5% were instilled in the left eye. The A-scan transducer was calibrated according to the manufacturer's instructions before each experiment. Five A-scan measurements were performed by touching the transducer to the cornea independently for each accommodative stimulus demand from 0 to 6.0 D in 1.0 D steps. To compensate for convergence, angular adjustment of the near target was performed by the subjects as described above for the UBM measurements. The ACD, lens thickness, vitreous chamber depth, and axial length were measured and corrected for the appropriate sound velocities.[26]

Objective Measurement of Accommodative Optical Response

Accommodative optical refractive changes were also independently, objectively measured in the same 24 subject eyes as a function of the same stimulus demands used for the UBM measurements. Those results will be reported in a separate paper.

Data Management and Analysis

All UBM image analysis data and A-scan data were stored in Matlab structures and saved as Matlab (.mat) files for later

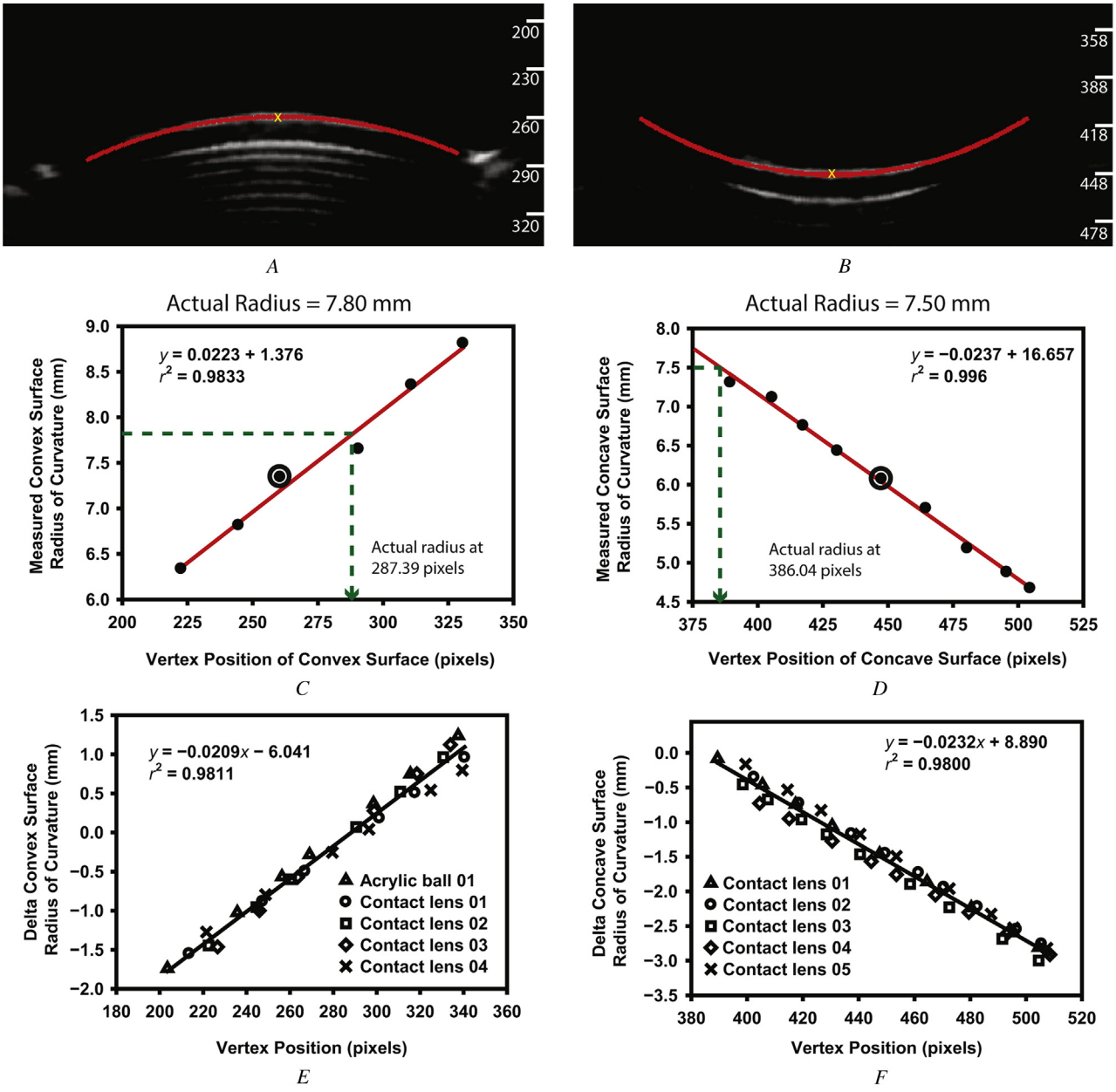

Figure 3. The UBM image analysis of a convex (*A*) and concave (*B*) calibration surface. The *y*-axis tick marks superimposed on the images represent the *y*-axis pixel positions in the UBM images. Comparison of the measured radius of curvature of the convex surface (C) and the concave surface (D) as a function of vertex distance. The circled points represent the 2 corresponding images in *A* and *B* above. The actual radius for the convex surface and the concave surface was calculated at vertex y-axis pixel positions of 287.39 and 386.04, respectively (*dashed lines*). Calibration functions for the convex (*E*) and concave (*F*) calibration surfaces. Note that *E* includes 1 acrylic ball and 4 contact lenses.

analysis. Matlab structures are a Matlab variable format for storing similar or disparate data types. From the UBM analysis, data were stored for corneal thickness, ACD, lens thickness, anterior segment length, anterior lens radius of curvature, posterior lens radius of curvature, ATA distance, pupil diameter, left anterior chamber angle, right anterior chamber angle, accommodative stimulus demand, image frame number, and image rotation angle. In addition, all identified pixel *x*- and *y*-coordinate positions for the lens anterior and posterior surfaces were stored in the Matlab structures. This provided the opportunity later to independently calculate the lens anterior and posterior radii of curvature for different entrance pupil diameters. This might be necessary because more pixels (representing a larger diameter) always were found for the lens anterior surface than for the lens posterior surface, and more pixels were found in the unaccommodated state than in the accommodated state because of accommodative pupil constriction. For each subject, all data for the above 15 analyzed parameters from each experiment were stored a single .mat file,

Table 2. Mean ± SD of root mean square error after calibration.

Calibration Surface	Mean ± SD of Root Mean Square Error	
	Radius (mm)	Power (D)*
Convex	0.21 ± 0.07	1.59 ± 0.38
Concave	0.16 ± 0.07	1.92 ± 1.05

*Calculated using the respective refractive index of each calibration surface

including all the analyzed data from 1050 images (7 stimulus demands × 3 trials × 50 images per video). The A-scan US measured ACD, lens thickness, vitreous chamber depth, and axial length were stored in a separate .mat file. A custom Matlab program was written to read these 2 files for the data analysis.

The default sound velocities used by the UBM and A-scan instruments were 1540 m/s and 1548 m/s, respectively. Sound velocity correction was applied to all measured parameters in accordance with accepted sound velocities for the ocular media (1660 m/s for the cornea, 1532 m/s for the aqueous and vitreous humor, and 1641 m/s for the crystalline lens).[26] Accommodative biometric stimulus-response functions for UBM-measured parameters were fit with linear regressions and second-order functions and tested for statistical significance. The UBM–measured accommodative biometric changes and the SDs were compared with the A-scan values. To assess the intrasession and intersession repeatability, for 8 subject eyes, the UBM and A-scan procedures were repeated once and for 10 subjects they were repeated twice. Repeatability analysis was performed using SPSS software (version 20.0, SPSS Inc.). Repeats were performed at least 5 days apart.

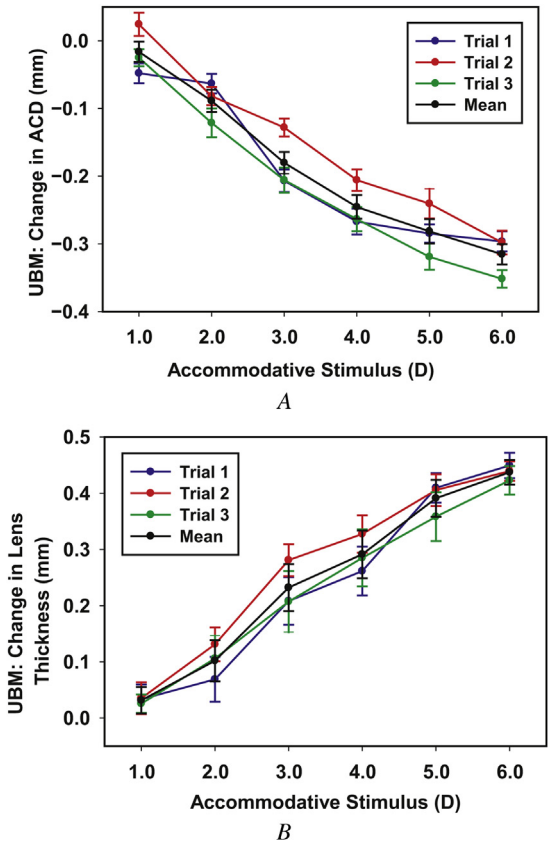

Figure 4. The UBM-measured ACD (*A*) and lens thickness (*B*) stimulus–response curves for the eye of 1 subject from 3 separate trials together with the mean. Error bars represent ± 1 SD from 150 measurements.

RESULTS

The study included 26 eyes of 26 subjects (8 men and 18 women) with a mean age of 24.15 years ± 3.03 (SD) (range 21 to 36 years). Because of the relatively low resolution of UBM images, the SDs of the measured parameters were analyzed. For the measured convex surface radii of curvature from a set of 50 images for all transducer distances for all calibration surfaces, the SDs ranged from 0.02 mm to 0.12 mm; for concave surface radii of curvature, the range was 0.01 to 0.12 mm. Table 2 shows the mean root-mean-square error for the convex and concave calibration surfaces after the UBM image calibration.

Of the 26 subject eyes studied, 16 were myopic (spherical refraction greater than −0.50 D) and 3 were hyperopic (spherical refraction +0.50 D or greater), with refractive errors ranging from −5.50 to +2.75 D (−1.31 ± 2.03 D).

Figure 4, *A* and *B*, shows 3, separate stimulus response functions of UBM-measured ACD and lens thickness from 1 eye.

Although objective accommodative optical changes were also independently measured in these eyes, that extensive data set will be discussed in a separate paper. In this paper, data are presented as a function of the accommodative stimulus demands. Because the accommodative amplitudes of all eyes were greater than the maximum stimulus demand (6.0 D), linear stimulus response relationships were expected for the parameters that change with accommodation. The numbers of eyes with statistically significant linear relationships between the accommodative stimulus demand and each anterior segment biometry parameter were 25 for ACD, 26 for lens thickness, 26 for anterior lens radius of curvature, 25 for posterior lens radius of curvature, and 13 for anterior segment length. Only data from eyes with statistically significant linear relationships between the accommodative stimulus and changes in biometry were included in the subsequent population plots (Figures 5, 6, 8*A*, and 10). Figure 5 shows the change in the UBM-measured ACD, lens thickness, anterior lens radius of curvature, posterior lens radius of curvature, and anterior segment length and the accommodative stimulus demand for this subject population. The population plots for these 5

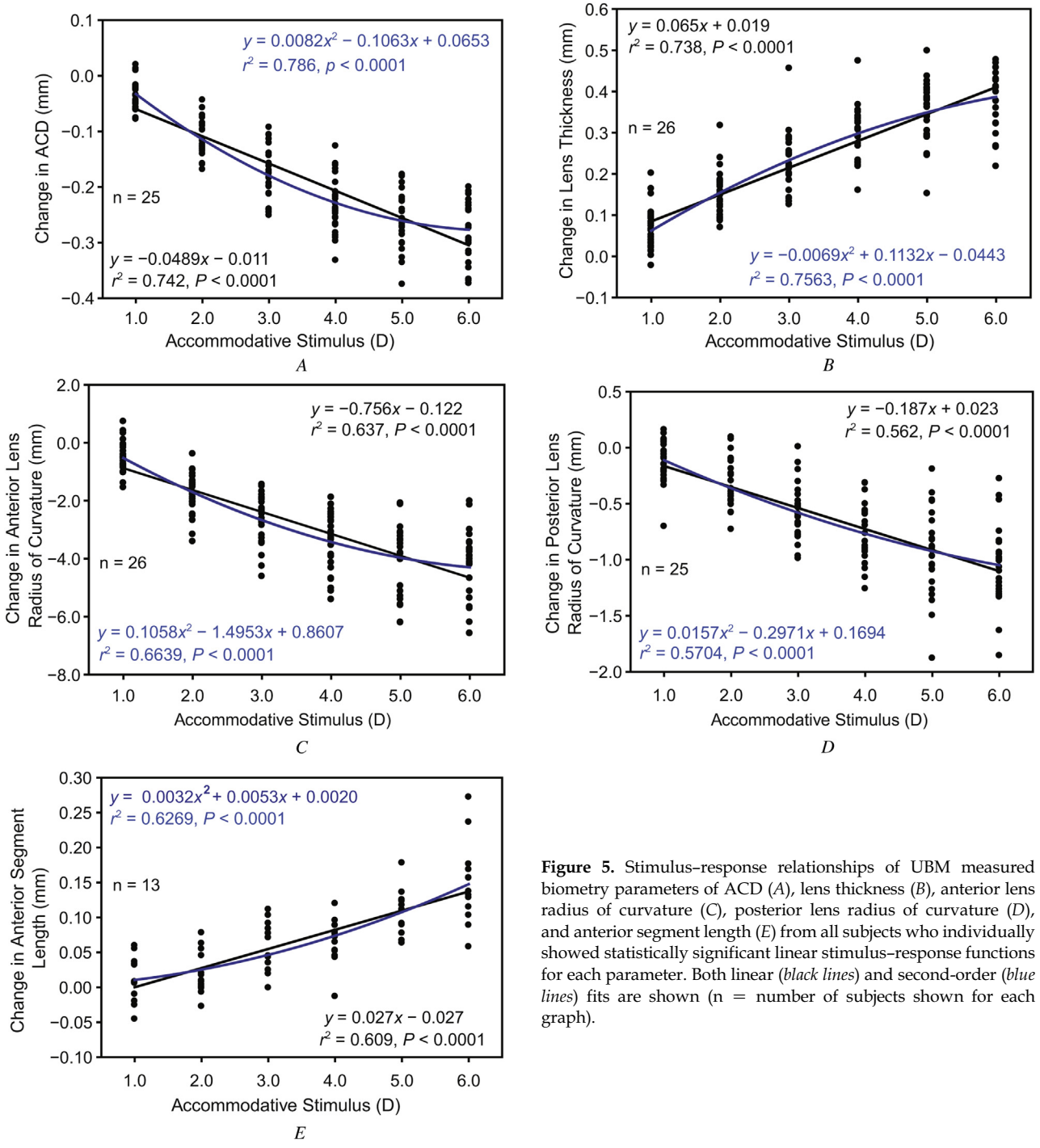

Figure 5. Stimulus–response relationships of UBM measured biometry parameters of ACD (*A*), lens thickness (*B*), anterior lens radius of curvature (*C*), posterior lens radius of curvature (*D*), and anterior segment length (*E*) from all subjects who individually showed statistically significant linear stimulus–response functions for each parameter. Both linear (*black lines*) and second-order (*blue lines*) fits are shown (n = number of subjects shown for each graph).

parameters were statistically significant fit with linear regression lines and with second-order lines ($P < .0001$), with only small improvements in the r^2 values for the second-order equations.

The linear regression line slopes represent the biometric changes per diopter of stimulus demand. Even though using per diopter values causes the per diopter accommodative biometric responses to be overestimated, previous accommodation biometry studies used them and so Table 3 uses them for like comparison with values from prior studies. Because various biometry parameters show statistically significant linear relationships with accommodative stimulus demands, they are expected to also be linearly related to each other. Figure 6 shows correlations between several of the anterior segment

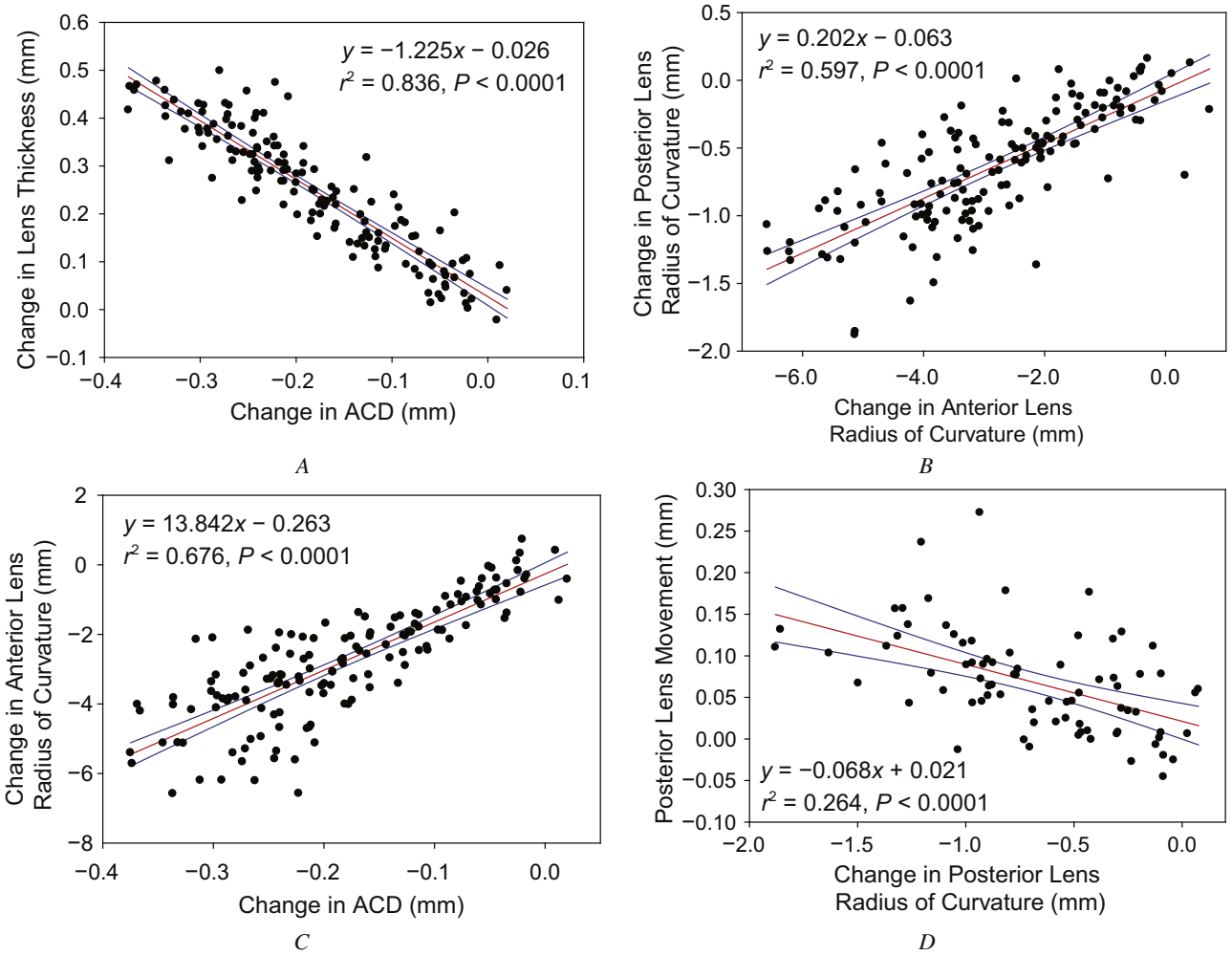

Figure 6. Linear relationships of change in (*A*) ACD versus lens thickness, (*B*) anterior lens radius of curvature versus posterior lens radius of curvature, (*C*) ACD versus anterior lens radius of curvature, and (*D*) posterior lens radius of curvature versus posterior lens surface movement ($P < .0001$) from all subjects. Linear regression parameters for other statistically significant biometry relationships are shown in Table 5 (*red lines* = linear regression, *blue lines* = 95% confidence interval).

biometry parameters that changed with accommodation. The correlations are tabulated in Figure 7.

The SD of the individual UBM parameters determined from the automated image analysis is indicative of the variance and resolution of the methods described. The SD of each of the measured biometry parameters was determined using 50 UBM images for each subject for each stimulus demand.

Change in Biometry		Horizontal Axis: ACD	LT	ALRC	PLRC
Vertical Axis	LT	−1.225, −0.026, 0.836*			
	ALRC	13.842, −0.263, 0.676	−9.925, −0.307, 0.633		
	PLRC	3.471, −0.012, 0.613	−2.571, 0.000, 0.621	0.202, −0.063, 0.597*	
	ASL	−0.330, 0.001, 0.316	0.339, −0.016, 0.569	−0.023, 0.002, 0.383	−0.068, 0.021, 0.264*

Figure 7. Linear regression parameters (each given as slope, intercept, and r^2, respectively) for comparison of UBM-measured anterior segment biometry parameters during accommodation. All regressions shown had statistically significant linear correlations ($P < .0001$) (ACD = anterior chamber depth; LT = lens thickness; ALRC = anterior lens radius of curvature; PLRC = posterior lens radius of curvature; ASL = anterior segment length). *Data plotted in Figure 6.

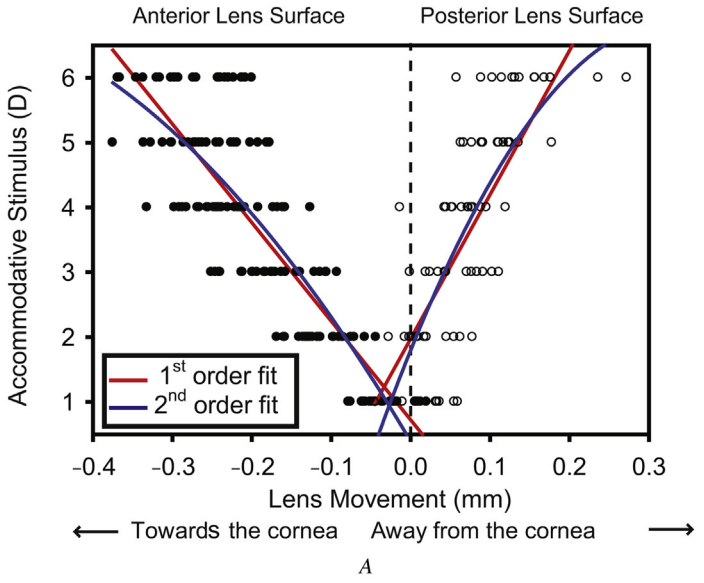

A

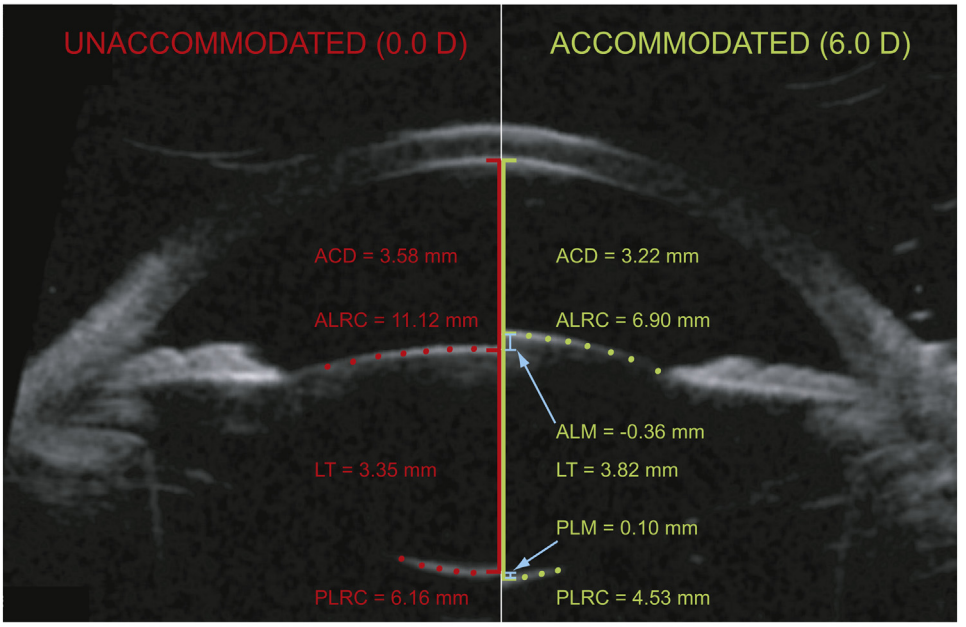

B

Figure 8. *A*: Lens surface movements as a function of accommodative stimulus ($P<.0001$ for both first- and second-order fits). The lens anterior surface moved anteriorly and the lens posterior surface moved posteriorly during accommodation. First- and second-order fits to the data are shown for comparison. *B*: Comparison of anterior segment biometric images for 1 subject from the unaccommodated state while viewing the far target (0 D, *left side*) and during the maximally accommodated state while viewing a 6.0 D target (*right side*). Only a subset of the pixels representing the lens surfaces are shown so the underlying image surfaces can be seen (ACD = anterior chamber depth; ALM = anterior lens surface movement; ALRC = anterior lens radius of curvature; LT = lens thickness; PLM = posterior lens surface movement; PLRC = posterior lens radius of curvature).

None of the measured parameter SDs showed statistically significant relationships with stimulus demand in any individual subject; therefore, the mean SD was calculated using the average SD of the measured biometry parameters from all subjects for all stimulus demands and trials (Table 4). The mean SD of the ACD, lens thickness, and anterior segment length for the population was less than 0.050 mm. The anterior lens radius of curvature, posterior lens radius of curvature, and pupil diameter had larger mean SDs. Corneal thickness, left anterior chamber angle, right anterior chamber angle, and ATA distance did not change statistically significantly during accommodation.

Pupil diameter was not included in the analysis because the automated image analysis algorithm consistently underestimated pupil diameters because of indistinct pupillary margins. The UBM image analysis was visually inspected to ensure that the identification of the anterior lens surface coordinates and calculation of the anterior lens radius of curvature did not include pixels belonging to the edges of the iris.

Figure 8, *A*, shows the anterior and posterior lens surface movement as a function of accommodative stimulus. As the accommodative stimulus demands increased, the anterior lens surface moved anteriorly linearly and the posterior lens surface moved

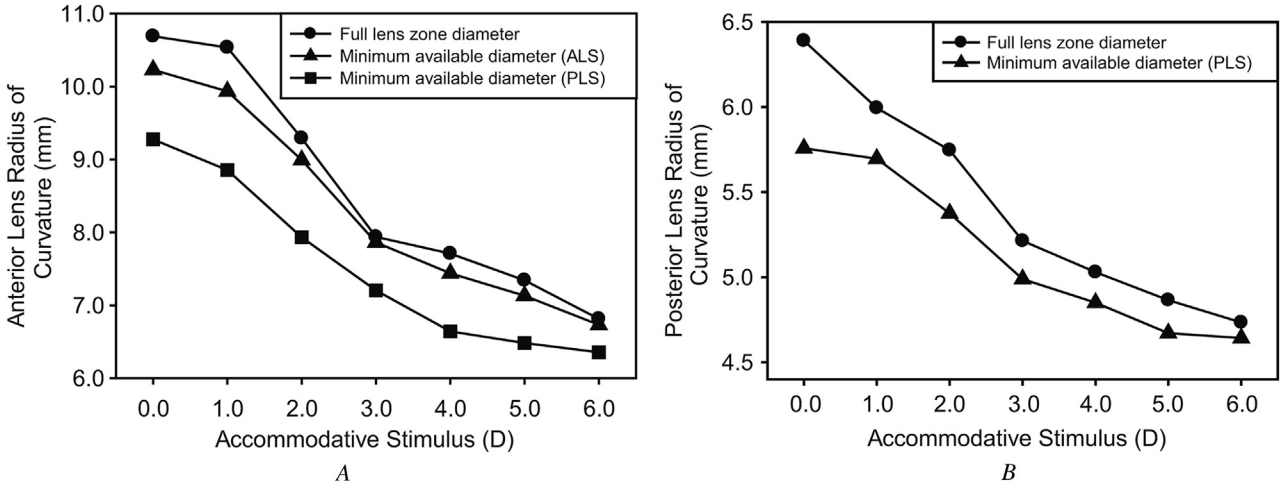

Figure 9. *A*: The anterior lens radius of curvature from 1 subject eye from a single trial for the full entrance pupil diameter available (the default analysis) (●), a minimum available lens zone diameter as determined from the maximally accommodated state pupil diameter for the anterior lens surface (ALS) (▲), and a minimum available lens zone diameter as determined from the posterior lens surface (PLS) (■) as a function of the accommodative stimulus. *B*: Posterior lens radius of curvature from the same eye for the full lens zone diameter available (●) and for the minimum available lens zone diameter from the maximally accommodated state as determined from the PLS (▲).

posteriorly linearly ($P < .0001$). The lens center as determined by the difference between the lens anterior and posterior vertices moved anteriorly during accommodation. In these eyes, the linear relationships show that the anterior lens surface movement and posterior lens surface movement contributed 70% and 30% of the change in lens thickness, respectively. Figure 8, *B*, compares the anterior segment biometry changes in the eye of a single subject in the unaccommodated and maximally accommodated states.

In the initial analysis of the images, the anterior and posterior lens radii of curvature were calculated by fitting circles to all pixels available for each lens surface. However, because the pupil constricts during accommodation, less lens surface is visible when the eye is accommodated and, because of the nature of the UBM signal, fewer pixels are available for the posterior lens surface (Figure 8, *B*). Therefore, using all the available pixels means that the circles are fit to more of the lens surface in the unaccommodated than in the accommodated state. Fitting a circle to fewer (or more) pixels could cause an underestimation (overestimation) of the radius of curvature. Having all available lens surface pixel coordinates stored made it possible to recalculate the anterior and posterior lens radii of curvature for the smallest available diameter (from the higher stimulus demands with smaller pupil diameters). Decreasing the diameter and the number of pixels considered resulted in a decrease in the anterior and posterior lens radii of curvature (Figure 9).

Intrasession repeatability analysis was performed on the UBM-measured ACD, lens thickness, anterior lens radius of curvature, posterior lens radius of curvature, and anterior segment length from 3 video sequences of all eyes for the 0 D stimulus demand. Intersession repeatability analysis was performed on the UBM-measured parameters for the 0 D stimulus demand for 18 eyes that had at least 1 repeat of the experiment. Intrasession and intersession repeatability was evaluated in terms of the coefficient of variation, which is the ratio of the SD of the measurements to the mean; the mean SD of the differences between the measurements; the coefficient of repeatability (CoR), which is 2 times the mean SD of the differences between the measurements; the CoR (%) which is the ratio of CoR to the mean of the measurements multiplied by 100; and the intraclass correlation coefficient (ICC). The ICC and other parameters in Table 5 show that the UBM parameters had a better intrasession repeatability than intersession repeatability.

Figure 10 compares UBM and A-scan US measurements of lens thickness (*A*) and ACD (*B*). There is a statistically significant linear correlation between the A-scan and UBM measurements of both parameters. The Bland-Altman plots in Figure 10 show the A-scan US underestimated the UBM-measured ACD by an average of 0.070 mm (*C*) and overestimated the UBM-measured lens thickness by an average of 0.166 mm (*D*).

The mean SDs of A-scan measured ACD and lens thickness were calculated in the same way as for UBM images (Table 4). There was no statistically significant relationship between the SDs of the A-scan measurements and the stimulus demand for any individual eye. The mean SDs of the A-scan ACD and lens

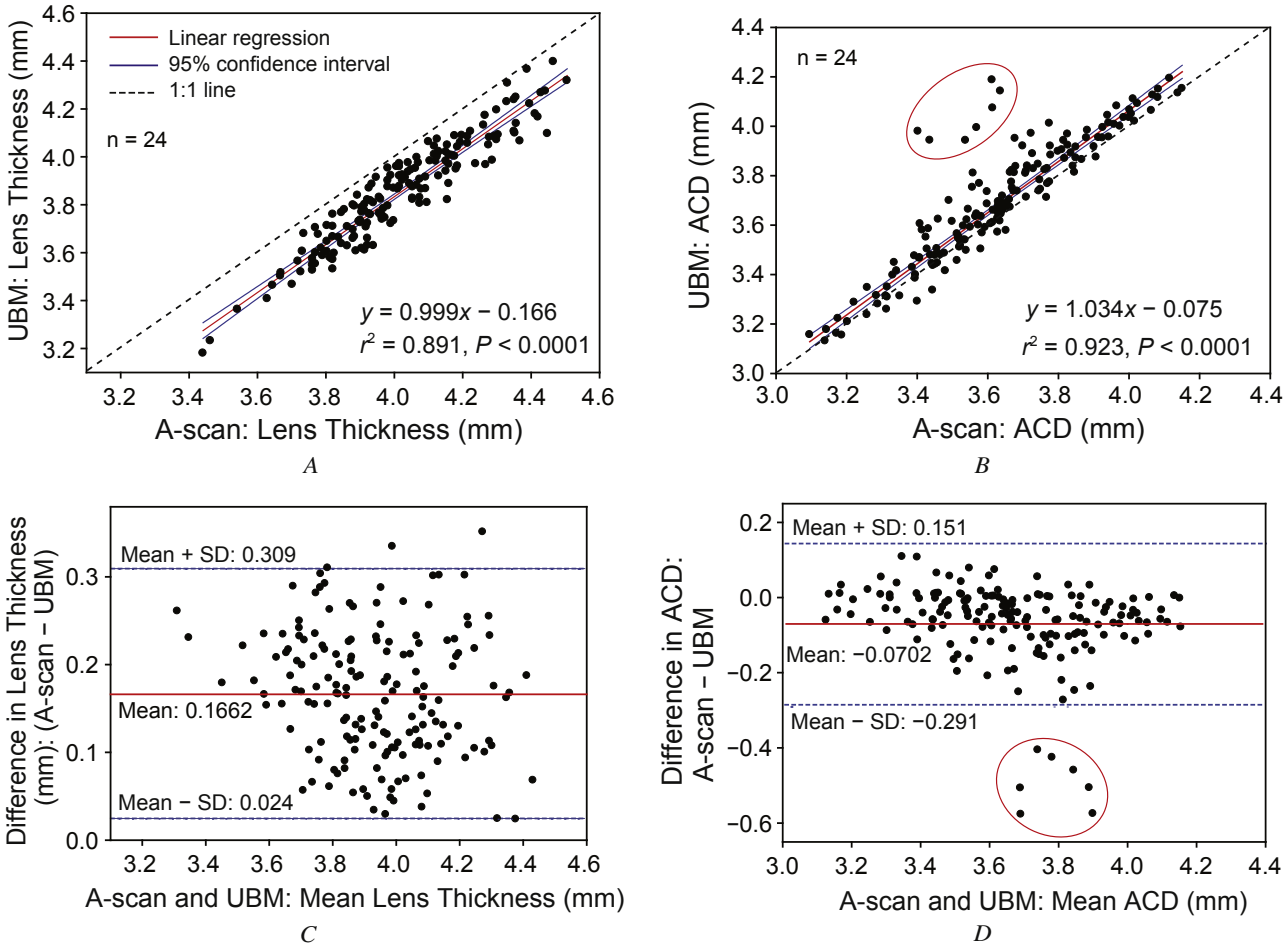

Figure 10. Linear correlation between A-scan US–measured and UBM-measured lens thickness (*A*) and ACD (*B*). Bland-Altman comparison of A-scan US–measured and UBM-measured lens thickness (*C*) and ACD (*D*). Appropriate corrections for sound velocity were applied for lens thickness and ACD measurements. Data points circled in red are from a single subject eye that showed an unusual response. The data from this 1 eye were not included in the regression calculations.

thickness measurements were calculated as the average SD of 5 measurements from all subjects for all stimulus demands and trials. Table 6 compares the SD of the A-scan and UBM measurements in the current study with the A-scan measurements from a previous study.[9]

DISCUSSION

Although objectively measured optical accommodative responses were also independently measured in this same subject population, because of the extensive data collected and analysis available, those results will be discussed in a separate article. Ideally, measured accommodative biometric changes would be compared with measured accommodative optical refractive changes to understand how accommodative biometry changes relate to refractive changes. However, because clinical accommodation testing can be demanding for patients, most clinical protocols choose to do one or the other. For this reason, in the present paper, the measured accommodative biometric changes were compared with the accommodative stimulus demands, not with the objectively measured accommodative optical responses.

In the present study, anterior segment biometry changes per diopter of stimulus demand were generally larger than per diopter of stimulus demand changes in previous studies[5,7,9,10,15,17–19] (Table 3). The differences between the present study and previous studies might be attributable to factors such as differences in the accommodative stimulus presentation, subject populations, sample size, imaging techniques, and subject posture (erect versus supine). Gravitational force from patient posture during measurements could affect how the lens moves during accommodation.[8,27] In the present study, the posterior accommodative movement of the posterior lens

Table 3. Per diopter of stimulus changes in biometry during voluntary accommodation in various human studies.

Study*	Biometry Method	Per-Diopter Changes in Biometry (mm)				
		ACD	LT	ALRC	PLRC	ASL
Ramasubramanian†	UBM	−0.049	+0.065	−0.756	−0.187	+0.027
Richdale[5]	OCT	N/A	+0.051	N/A	N/A	N/A
Jones[7]	MRI	N/A	+0.050	N/A	N/A	N/A
Dubbelman[9]	Scheimpflug	−0.038	+0.045	−0.620	−0.130	+0.008
Brown[10]	Photography	−0.030	+0.045	−0.545	−0.371	+0.015
Tsorbatzoglou[15]	PCI	−0.027	+0.036	N/A	N/A	N/A
Garner[17]	A-scan	−0.033	+0.040	N/A	N/A	+0.007
Shum[18]	A-scan	−0.035	+0.053	N/A	N/A	N/A
Beauchamp[19]	A-scan	−0.037	+0.056	N/A	N/A	+0.022

ACD = anterior chamber depth; ALRC = anterior lens radius of curvature; ASL = anterior segment length; LT = lens thickness; MRI = magnetic resonance imaging; N/A = not available; OCT = optical coherence tomography; PCI = partial coherence interferometry; PLRC = posterior lens radius of curvature; UBM = ultrasound biomicroscopy
*First author
†Present study

surface is in agreement with results from several earlier studies,[2,4,19] but not with an MRI study.[8] Possibly, this is not seen in MRI images because of limited MRI resolution.[8] The percentage contribution of the lens surface movements to the overall increase in lens thickness is comparable to values reported in previous human[3,4,15,19] and monkey[2,28] studies.

The SDs of the measured UBM biometry parameters reported here are considerably smaller than in previous UBM,[20,21] A-scan US,[3] and OCT[22] studies, and even than in a previous PCI study (which has considerably higher resolution than UBM).[4] The SD calculated from automated analysis of a sequence of 50 UBM images does not include variability caused by multiple independent measurements in which ocular alignment with the instrument can change with each repeated measure. However, the SDs calculated here (Table 4) do include all possible sources of variability in that they are from all subjects and all stimulus demands and from 2 repeats. Although the SD is calculated from many measurements, increasing the number of measurements does not reduce the SD but rather yields a more robust estimate. Factors such as eye movement, the UBM transducer position and stability, the position of the plane of best focus of the UBM, physiological variations of biometry between trials, the tilt of the transducer, and the scanning location in the eye can affect the variance of biometry measurements. These possible contributing factors also could apply to A-scan US data.

Table 4. Mean SD of the UBM–measured biometry parameters.

Parameter	Mean SD ± SD
Changed during accommodation	
Anterior chamber depth (mm)	0.017 ± 0.003
Lens thickness (mm)	0.029 ± 0.007
Anterior lens radius of curvature (mm)	0.335 ± 0.138
Posterior lens radius of curvature (mm)	0.158 ± 0.038
Anterior segment length (mm)	0.034 ± 0.009
Pupil diameter (mm)	0.265 ± 0.130
Unchanged during accommodation	
Corneal thickness (mm)	0.012 ± 0.003
Angle-to-angle distance (mm)	0.081 ± 0.022
Left anterior chamber angle (degrees)	4.3 ± 1.7
Right anterior chamber angle (degrees)	4.7 ± 1.9

The SDs of the UBM-measured anterior and posterior lens radii of curvatures were larger than for the other parameters. This is likely attributable to the limited number of lens surface pixels used to fit a circle, which is limited by the pupil diameter. The anterior and posterior lens surfaces in the UBM images are indistinct, which adds further variability. Dilation of the iris with phenylephrine could improve measurements of the lens surface curvatures without affecting accommodation.[29] Of all the measured biometry parameters, most of the accommodative change in power of the phakic lens comes from the changes in lens surface curvature during accommodation.[30] Moreover, the surfaces of the anterior and posterior lens are aspheric. Fitting the surface coordinates with a spherical equation might not represent the true geometry of the lens surface; however, the resolution of the UBM images and the data available from the lens surfaces precludes meaningful analysis using aspheric fits.

In the present study, UBM and A-scan measurements were performed independently; therefore, measurement differences are expected if subjects do not accommodate the same amount for both

Table 5. Intrasession and intersession repeatability for UBM-measured parameters.

	Parameter				
Repeatability	CoV	Mean SD of Differences (mm)	CoR	CoR (%)	ICC
Intrasession (n = 26)					
Anterior chamber depth	0.005	0.020	0.040	1.183	0.994
Lens thickness	0.008	0.026	0.052	1.433	0.985
ALRC	0.032	0.301	0.602	5.193	0.949
PLRC	0.026	0.108	0.216	3.860	0.960
Anterior segment length	0.006	0.039	0.077	1.034	0.975
Central corneal thickness	0.022	0.005	0.009	1.711	0.984
Intersession (n = 18)					
Anterior chamber depth	0.005	0.025	0.050	1.486	0.989
Lens thickness	0.008	0.021	0.043	1.164	0.987
ALRC	0.032	0.434	0.869	7.126	0.828
PLRC	0.026	0.117	0.235	4.101	0.939
Anterior segment length	0.006	0.038	0.076	1.004	0.957
Central corneal thickness	0.022	0.004	0.009	1.627	0.985

ALRC = anterior lens radius of curvature; CoR = coefficient of repeatability; CoR (%) = the ratio of the CoR to the mean of the measurements multiplied by 100; CoV = coefficient of variation; ICC = intraclass correlation coefficient; PLRC = posterior lens radius of curvature

measurements (Figure 10). However, if on average both instruments measure the same accommodative changes, the Bland-Altman plots should show an average difference of zero. The source of the systematic difference in lens thickness between UBM and A-scan is unclear. The SDs for UBM-measured ACDs and lens thickness were smaller than for A-scan measurements. This might be attributable to the stable positioning and alignment of the UBM transducer achievable by viewing the live UBM image on the monitor.

Differences within the subject groups, in the examiner, and in the subject's posture could account for smaller A-scan SDs for ACD and lens thickness in the present study than in a previous study.[3] Assuming that A-scan US is the gold standard, the mean correction factor for the UBM-measured ACD and lens thickness was calculated to match, on average, the A-scan measurements. Ratios of A-scan and UBM measurements of ACD and lens thickness were calculated for 24 subjects for 7 stimulus demands (0 to 6.0 D) to yield 168 correction factors. The mean ± SD of all these ratios was 0.982 ± 0.03 and 1.044 ± 0.02, respectively, for ACD and lens thickness. Multiplying the UBM measurements by the ratios would, on average, get the UBM measurements in agreement with the A-scan measurements.

Table 6. Mean SD ± SD for ACD and lens thickness during accommodation in the present study and a previous study.[9]

	Current Study		Previous Study[9]
Biometry	UBM*	A-Scan*	A-Scan†
ACD	0.017 ± 0.003	0.041 ± 0.024	0.135
LT	0.029 ± 0.007	0.039 ± 0.022	0.115

ACD = anterior chamber depth; LT = lens thickness; UBM = ultrasound biomicroscopy
*Mean SD ± SD (mm)
†Mean SD (mm)

The automated Matlab image analysis program used in the present study enabled objective measurement of the UBM image sequences. Image analysis programs such as this might be useful if they can be incorporated in the commercially available UBM software to perform real-time image analysis. Visualizing the accommodative anterior segment changes and performing real-time objective measurements of biometry might be useful for understanding the accommodative mechanism and for designing and evaluating accommodating IOLs. Clinicians might also use real-time image analysis in the preoperative assessment of presbyopic eyes and to quantify movement of an accommodating IOL in pseudophakic eyes. If the correlations between ocular accommodative biometric changes and objectively measured optical accommodative responses are strong, it might also be possible to reasonably accurately predict the accommodative optical response of an eye using the measured accommodative biometric changes.

In conclusion, this study has demonstrated the usefulness of automated image analysis to perform objective measurement of the accommodative biometric changes from UBM image sequences. The SD of the

UBM-measured biometry parameters from automated image analysis is considerably smaller than reported in previous UBM and A-scan studies. The UBM-measured accommodative anterior segment biometry parameters have smaller variance and good repeatability. The radius of curvature of intraocular structures calculated from UBM images requires distortion correction. With automated objective measurements, UBM can be a useful commercially available clinical tool for accommodation studies.

WHAT WAS KNOWN

- Previous studies have measured accommodative biometric changes from UBM images using manual analysis methods. Limitations of these studies include larger variance of measurements, insufficient number of images used for analysis, and possible measurement bias.

WHAT THIS PAPER ADDS

- Objectively measured UBM accommodative anterior segment biometry parameters had smaller variance and good repeatability.
- Spatial distortions present in UBM images can be corrected to obtain quantitative measurements of accommodative changes in crystalline lens surface radii of curvature.

REFERENCES

1. Helmholtz H. Mechanism of accommodation. In: Southall JPC, ed, Helmholtz's Treatise on Physiological Optics, translated from the third German edition. New York, NY, Dover, 1962; volume 1, 143–173
2. Vilupuru AS, Glasser A. The relationship between refractive and biometric changes during Edinger-Westphal stimulated accommodation in rhesus monkeys. Exp Eye Res 2005; 80:349–360
3. Ostrin L, Kasthurirangan S, Win-Hall D, Glasser A. Simultaneous measurements of refraction and A-scan biometry during accommodation in humans. Optom Vis Sci 2006; 83:657–665. Available at: http://journals.lww.com/optvissci/Fulltext/2006/09000/Simultaneous_Measurements_of_Refraction_and_A_Scan.10.aspx. Accessed November 18, 2014
4. Bolz M, Prinz A, Drexler W, Findl O. Linear relationship of refractive and biometric lenticular changes during accommodation in emmetropic and myopic eyes. Br J Ophthalmol 2007; 91:360–365. Available at: http://www.ncbi.nlm.nih.gov/pmc/articles/PMC1857649/pdf/360.pdf. Accessed November 18, 2014
5. Richdale K, Bullimore MA, Zadnik K. Lens thickness with age and accommodation by optical coherence tomography. Ophthalmic Physiol Opt 2008; 28:441–447. Available at: http://www.ncbi.nlm.nih.gov/pmc/articles/PMC2857534/pdf/nihms192832.pdf. Accessed November 18, 2014
6. Glasser A, Wendt M, Ostrin L. Accommodative changes in lens diameter in rhesus monkeys. Invest Ophthalmol Vis Sci 2006; 47:278–286. Available at: http://www.iovs.org/cgi/reprint/47/1/278.pdf. Accessed November 18, 2014
7. Jones CE, Atchison DA, Pope JM. Changes in lens dimensions and refractive index with age and accommodation. Optom Vis Sci 2007; 84:990–995. Available at: http://journals.lww.com/optvissci/Fulltext/2007/10000/Changes_in_Lens_Dimensions_and_Refractive_Index.15.aspx. Accessed November 18, 2014
8. Kasthurirangan S, Markwell EL, Atchison DA, Pope JM. MRI study of the changes in crystalline lens shape with accommodation and aging in humans. J Vis 2011; 11(3):1–16. Available at: http://www.journalofvision.org/content/11/3/19.full.pdf. Accessed November 18, 2014
9. Dubbelman M, van der Heijde GL, Weeber HA. Change in shape of the aging human crystalline lens with accommodation. Vision Res 2005; 45:117–132
10. Brown N. The change in shape and internal form of the lens of the eye on accommodation. Exp Eye Res 1973; 15:441–459
11. Sheppard AL, Evans CJ, Singh KD, Wolffsohn JS, Dunne MCM, Davies LN. Three-Dimensional Magnetic Resonance Imaging of the Phakic Crystalline Lens during Accommodation. Invest Ophthalmol Vis Sci 2011; 52:3689–3697. Available at: http://www.iovs.org/content/52/6/3689.full.pdf. Accessed November 18, 2014
12. Glasser A, Kaufman PL. The mechanism of accommodation in primates. Ophthalmology 1999; 106:863–872
13. Koretz JF, Cook CA, Kaufman PL. Accommodation and presbyopia in the human eye; changes in the anterior segment and crystalline lens with focus. Invest Ophthalmol Vis Sci 1997; 38:569–578. Available at: http://www.iovs.org/cgi/reprint/38/3/569.pdf. Accessed November 18, 2014
14. Koeppl C, Findl O, Kriechbaum K, Drexler W. Comparison of pilocarpine-induced and stimulus-driven accommodation in phakic eyes. Exp Eye Res 2005; 80:795–800
15. Tsorbatzoglou A, Németh G, Szél N, Biró Z, Berta A. Anterior segment changes with age and during accommodation measured with partial coherence interferometry. J Cataract Refract Surg 2007; 33:1597–1601
16. Koretz JF, Bertasso AM, Neider MW, True-Gabelt BA, Kaufman PL. Slit-lamp studies of the rhesus monkey eye: II. Changes in crystalline lens shape, thickness and position during accommodation and aging. Exp Eye Res 1987; 45:317–326
17. Garner LF, Yap MKH. Changes in ocular dimensions and refraction with accommodation. Ophthalmic Physiol Opt 1997; 17:12–17
18. Shum PJ-T, Ko L-S, Ng C-L, Lin S-L. A biometric study of ocular changes during accommodation. Am J Ophthalmol 1993; 115:76–81
19. Beauchamp R, Mitchell B. Ultrasound measures of vitreous chamber depth during ocular accommodation. Am J Optom Physiol Opt 1985; 62:523–532
20. Modesti M, Pasqualitto G, Appolloni R, Pecorella I, Sourdille P. Preoperative and postoperative size and movements of the lens capsular bag: ultrasound biomicroscopy analysis. J Cataract Refract Surg 2011; 37:1775–1784
21. Marchini G, Pedrotti E, Sartori P, Tosi R. Ultrasound biomicroscopic changes during accommodation in eyes with accommodating intraocular lenses; pilot study and hypothesis for the mechanism of accommodation. J Cataract Refract Surg 2004; 30:2476–2482
22. Sun Y, Fan S, Zheng H, Dai C, Ren Q, Zhou C. Noninvasive imaging and measurement of accommodation using dual-channel SD-OCT. Curr Eye Res 2014; 39:611–619
23. Siedlecki D, de Castro A, Gambra E, Ortiz S, Borja D, Uhlhorn S, Manns F, Marcos S, Parel J-M. Distortion correction of OCT images of the crystalline lens: gradient index approach. Optom Vis Sci 2012; 89(5):E709–E718. Available at: http://www.ncbi.nlm.nih.gov/pmc/articles/PMC3348411/pdf/nihms-364764.pdf. Accessed November 18, 2014

24. Ishikawa H, Liebmann JM, Ritch R. Quantitative assessment of the anterior segment using ultrasound biomicroscopy. Curr Opin Ophthalmol 2000; 11:133–139
25. Nakatsuka C, Hasebe S, Nonaka F, Ohtsuki H. Accommodative lag under habitual seeing conditions: comparison between adult myopes and emmetropes. Jpn J Ophthalmol 2003; 47:291–298
26. Jansson F, Sundmark E. Determination of the velocity of ultrasound in ocular tissues at different temperatures. Acta Ophthalmol (Copenh) 1961; 39:899–910
27. Tromans C, Storey JK. Biometric investigation of the effect of gravity on the crystalline lens during accommodation. Doc Ophthalmol Proc Ser 1990; 53:125–129
28. Vilupuru AS, Glasser A. Dynamic accommodative changes in Rhesus monkey eyes assessed with A-scan ultrasound biometry. Optom Vis Sci 2003; 80:383–394. Available at: http://journals.lww.com/optvissci/Fulltext/2003/05000/Dynamic_Accommodative_Changes_in_Rhesus_Monkey.13.aspx. Accessed November 18, 2014
29. Richdale K, Bailey MD, Sinnott LT, Kao CY, Zadnik K, Bullimore MA. The effect of phenylephrine on the ciliary muscle and accommodation. Optom Vis Sci 2012; 89:1507–1511. Available at: http://journals.lww.com/optvissci/Fulltext/2012/10000/The_Effect_of_Phenylephrine_on_the_Ciliary_Muscle.12.aspx. Accessed November 18, 2014
30. Maceo BM, Manns F, Borja D, Nankivil D, Uhlhorn S, Arrieta E, Ho A, Augusteyn RC, Parel J-M. Contribution of the crystalline lens gradient refractive index to the accommodation amplitude in non-human primates: in vitro studies. J Vis 2011; 11(13):23. Available at: http://www.journalofvision.org/content/11/13/23.full.pdf. Accessed November 18, 2014

First author:
Viswanathan Ramasubramanian, PhD

College of Optometry, University of Houston, Houston, Texas, USA